Available online at www.sciencedirect.com
ScienceDirect
International Journal of Mass Spectrometry 260 (2007) 128–136
International Journal of Mass Spectrometry
www.elsevier.com/locate/ijms

Molecular imaging of lipids in cells and tissues

Katrin Börner [a], Per Malmberg [a], Jan-Eric Månsson [b], Håkan Nygren [a,*]

[a] *Institute of Biomedicin, Department of Medical Biochemistry and Cell Biology, The Sahlgrenska Academy at Göteborg University, Sahlgrenska University Hospital, SE-405 30 Göteborg, Sweden*
[b] *Institute of Neuroscience and Physiology, Department of Psychiatry and Neurochemistry, The Sahlgrenska Academy at Göteborg University, Sahlgrenska University Hospital, SE-431 80 Mölndal, Sweden*

Received 31 May 2006; received in revised form 29 August 2006; accepted 8 September 2006
Available online 2 October 2006

Abstract

The distribution pattern of lipid species in biological tissues was analyzed with imaging mass spectrometry (TOF-SIMS; time-of-flight secondary ion mass spectrometry). The first application shows distribution of a glycosphingolipid, the galactosylceramide-sulfate (sulfatide) with different hydrocarbon chain lengths and the fatty acids palmitate and oleate in rat cerebellum. Sulfatides were seen localized in regions suggested as paranodal areas of rat cerebellar white matter as well as in the granular layer, with highest concentrations at the borders of the white matter. Different distribution patterns could be shown for the fatty acid C16:0 palmitate and C18:1 oleate in rat cerebellum, which seem to origin partly from the hydrocarbon chains of phosphatidylcholine. Results were shown for two different tissue preparation methods, which were plunge-freezing and cryostat sectioning as well as high-pressure freezing, freeze-fracturing and freeze-drying.

The second application shows TOF-SIMS analysis on a biological trial of choleratoxin treatment in mouse intestine. The effect of cholera toxin on lipids in the intestinal epithelium was shown by comparing control and cholera toxin treated mouse intestine samples. A significant increase of the cholesterol concentration was seen after treatment. Cholesterol was mainly localized to the brush border of enterocytes of the intestinal villi, which could be explained by the presence of cholesterol-rich lipid rafts present on the microvilli or by relations to cholesterol uptake. After cholera toxin exposure, cholesterol was seen increased in the nuclei of enterocytes and apparently in the interstitium of the villi.

We find that imaging TOF-SIMS is a powerful tool for studies of lipid distributions in cells and tissues, enabling the elucidation of their role in cell function and biology.

Keywords: Galactosylceramide-sulfate; Cholesterol; Palmitate; Oleate; TOF-SIMS

1. Introduction

Lipids display a wide diversity in cell metabolics and biochemistry, as they are involved in energy production and storage, signal transduction and the formation of the permeability barrier of cells and organells in form of a lipid bilayer [1]. Therefore, studies on lipid heterogenity and composition, as for example in protein–lipid interactions, membrane structure or lipid domains, are of great interest and give information about specific physiological functions in different tissues and cells. Common methods that are used successfully in lipid analysis are chromatography methods, e.g., HPLC, thin layer chromatography, high-precision gas chromatography together with ionization techniques and mass spectrometry, which give detailed information on lipid quality and quantity [2,3]. These methods require lipid extraction from a defined tissue matrix, which limits information of lipid localization to the areas chosen or which are defined by separation of specific cell types. Imaging of specific lipids with antibodies is difficult, but some efforts have been made with synthesized fluorescent labelled lipids [4,5].

Imaging mass spectrometry has so far shown to be a promising alternative in imaging lipids. Results could be shown on different classes of lipids and fatty acids: phospholipid distribution pattern were shown in cell cultures [6,7] and tissue slices [8–11], as well as distributions of sphingolipids [12], fatty acids [8,13], cholesterol [9,11,14,15] and other [8,16].

Time-of-flight secondary ion mass spectrometry (TOF-SIMS) is a technique allowing identification and localization of all elements and detection of all isotopes and imaging with

* Corresponding author. Tel.: +46 31773 3385; fax: +46 31773 3330.
E-mail address: hakan.nygren@anatcell.gu.se (H. Nygren).

1387-3806/$ – see front matter © 2006 Elsevier B.V. All rights reserved.
doi:10.1016/j.ijms.2006.09.014

excellent spatial resolution [17]. These qualities should make the method ideal for analysis of biological samples, and several attempts have been made in that direction [18]. A major obstacle has been that the TOF-SIMS analysis is based on the outcome of the impact of a high-energy primary ion onto a target sample and the yield of large molecular weight fragments, necessary for the identification of the original molecule, may be limited. A successful approach, yielding ion desorption of large fragments is the use of gold clusters as primary ion source [19]. Along this line, the advent of the bismuth cluster ion source [20] is a major leap in progress of TOF-SIMS analysis of bio-samples due to its high yields of secondary ions [13]. TOF-SIMS has an ultra-high sensitivity to surface layers, in atomic concentrations as low as 10 ppm. The distribution of organics and non-organics can be measured concomitant for the same sample, e.g., one cell compartment or tissue section. The mass spectrometer provides the possibility to investigate a wide mass range with high sensitivity and a quasi-simultaneous detection of all secondary ions.

Another important factor in bioimaging mass spectrometry is the effect of tissue preservation and handling on the results of the analysis. Imaging mass spectrometry is, in relation to fluorescence microscopy and other established histochemical techniques, not depending on the use of specific probes, their penetration into the sample and reactivity with their target. So far, tissue fixation with fast freezing is the method of choice, with plunge-freezing the cells or tissue segments or high-pressure freezing, avoiding chemical alterations and freezing the tissue to immobilize the molecules at their original sites of localization. In this work, histological localization of lipid species and fatty acids from two tissue samples were presented with both sample preparation methods.

2. Material and methods

2.1. Animals and tissue preparation

2.1.1. Cholera toxin treatment of mouse intestine

Adult Balb/c mice, 12–14 weeks old, were used, fasting over night before treatment. The mice were deeply anaesthetized with isoflurane (Baxter Medical AB, Kista, Sweden) and cholera toxin (List Biological Laboratories Inc.) was administered by gavages in a 300 μl solution consisting of 125 μl phosphate-buffered solution (PBS), 150 μl bicarbonate solution (3% $NaHCO_3$ in PBS) and 25 μl cholera toxin. Control mice did not receive cholera toxin treatment. The mice had free access to water everytime and food was regiven directly after feeding. After 8 h, the treated mice and control mice were euthanized with CO_2 and cervical dislocation. About 2 cm of mouse duodenum were dissected and the chyme was ejected by carefully squeezing the tissue into one direction.

2.1.2. Rat cerebellum

Male Sprague–Dawley rats (300 g) were deeply anaesthetized with Isofluran Baxter (Baxter Medical AB, Kista, Sweden) and sacrificed under anaesthesia. The skin was removed and the cranium opened carefully. The cerebellum was dissected by transection of the connections with pons and medulla oblongata. The cerebellar hemispheres were separated from the vermis.

2.2. Tissue preparation

2.2.1. Procedure 1

Tissue samples were cut in smaller blocks of about 3–4 mm in diameter which were directly plunge frozen in liquid nitrogen. The frozen tissue was cut with a Leica cryostat at −23 °C in slices of 8–25 μm thickness. The slices were placed onto an object slide and dried at room temperature. Until measurement with TOF-SIMS, the samples were kept dry in a desiccator under vacuum.

2.2.2. Procedure 2

The cerebellum was dissected by transection of the connections with pons and medulla oblongata. All further steps were carried out under cold conditions, keeping the tissue in ice-cold phosphate buffered saline (PBS), 0.05 M phosphate buffer pH 7.4. The dura mater was removed and the cerebellum hemispheres were dissected under a stereomicroscope. The hemispheres were glued onto a vibratome sample holder with Roti®coll tissue glue and immediately embedded in 3% Agar noble when it was almost hardened. For vibratome cutting (Leica, VT1000S), we filled the ice-cooled chamber with cold PBS and mounted the sample holder with the embedded tissue in the instrument. A slice of 900 μm thickness was cut with the vibratome and discarded. Then, the tissue was cut in 300–350 μm thick slices, which were used for high-pressure freezing.

2.2.3. High-pressure freezing of cerebellum samples

High-pressure freezing was accomplished with the EMPACT (Leica, Vienna) at 2000 bar and −196 °C, as described in detail by others [21]. As soon as a vibratome section was cut, smaller tissue samples of 1.2 mm in diameter were punched out. Regions for punching were chosen from the outer regions of the white matter in the cerebellum arbor vitae. The outermost cell layers of the slice were excluded to avoid possible embedding or chemical artefacts from this region. The punched tissue was placed onto the freeze-fracture carrier under a stereomicroscope. Excess PBS was removed with a filter paper and the copper ring was put on top of the loaded carrier. With help of the loading station, the sample was inserted into the instrument. After cryofixation, the carriers were collected in the liquid nitrogen bath of the EMPACT.

2.2.4. Freeze-fracturing and freeze-drying of the frozen samples

The samples were quickly transferred onto a pre-cooled copper block in liquid nitrogen. With help of a pair of forceps, the copper ring was removed from the carrier to lay open a fractured surface. The sample was inserted into a vacuum chamber and freeze-dried over night at 10^{-3} mbar [22]. The samples were kept in a desiccator under vacuum until TOF-SIMS measurements.

2.3. Reference samples

Phosphocholine and oleate acid reference samples, grade >99, were purchased from Sigma–Aldrich, Stockholm, Sweden. The galactosylceramide-sulfate reference sample was prepared from bovine brain and characterized as described previously [23,24]. The reference samples were dissolved in C/M/W (C, chloroform; M, methanol; W, water; 30:60:20, v/v/v) at a concentration of 100 pM and prepared by droplet deposition onto clean aluminum foil before mass spectrometry. Surface spectra were taken as described below.

2.4. TOF-SIMS analysis

Measurements were perfomed at Tascon GmbH, Münster, Germany, under commercial conditions. The tissue sections were analyzed with a TOF-SIMS mass spectrometer, IONTOF TOF-SIMS IV and IONTOF TOF-SIMS 5 instruments. Both instruments were equipped with a Bi^{3+} liquid metal ion gun (Bi^{3+} LMIG). First, surface spectra were taken from an area of 100 μm × 100 μm in order to identify the species present at the respective surfaces. Here, the bunched mode was used (high mass resolution, 3 μm lateral resolution). Bi^{3+} primary ions were

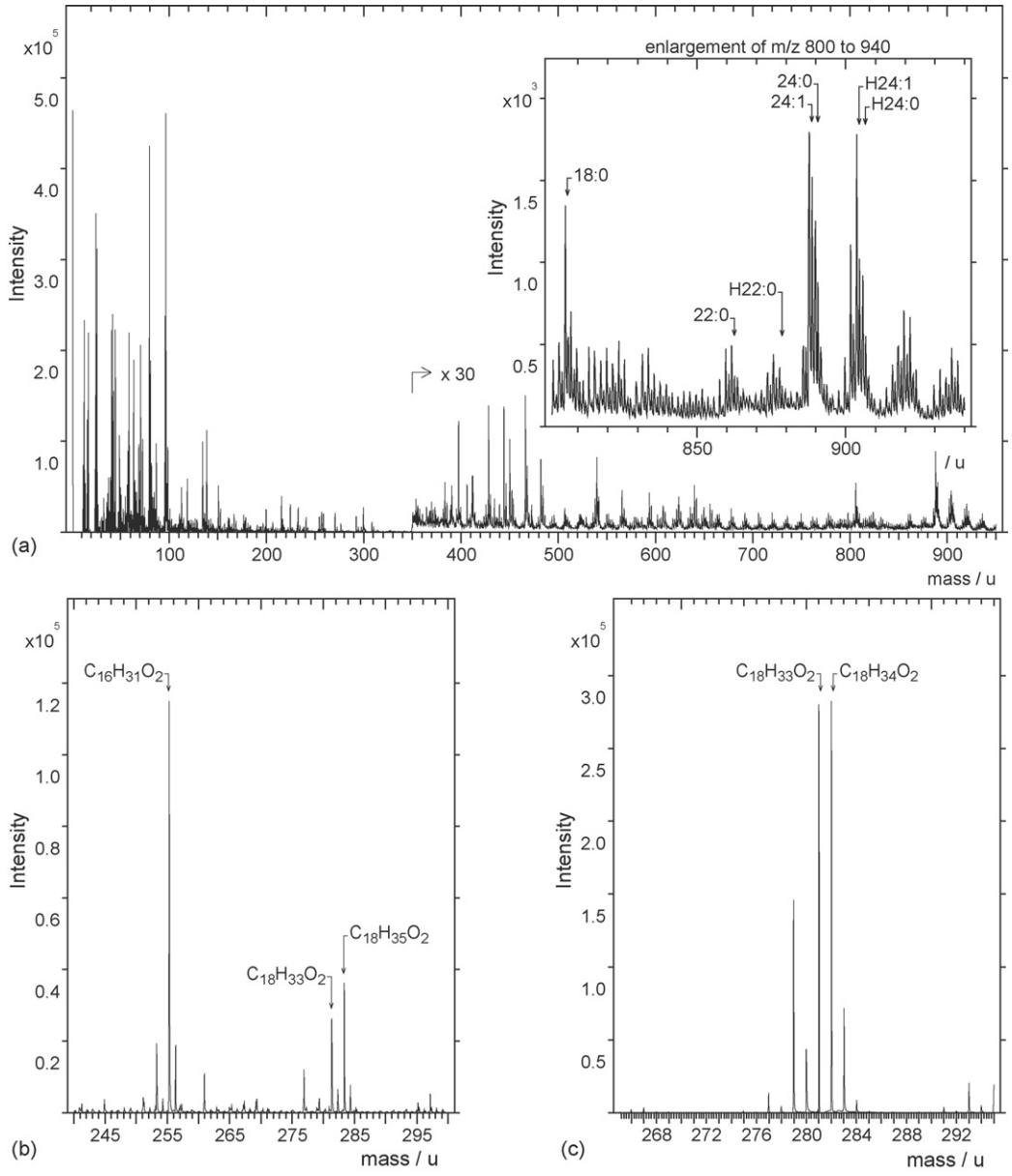

Fig. 1. (a) Negative TOF-SIMS spectrum of sulfatide reference samples showing peaks for different galactosylceramide-sulfates with chain length of C18:0 at *m/z* 806.6, C22:0 at *m/z* 862.6, CH22:0 at *m/z* 878.6, C24:1 at *m/z* 888.6, C24:0 at *m/z* 890.6 and CH24:0 at *m/z* 906.6. (b) Negative TOF-SIMS spectrum of the reference sample for phosphatidylcholine, showing a spectra enlargement from *m/z* 240 to *m/z* 300 which point to specific peaks at *m/z* 255.2 for, the palmitate fatty acid constituent of phosphatidylcholine $C_{16}H_{31}O_2$ $[M-H]^-$, a peak at *m/z* 281.2 for $C_{18}H_{33}O_2$ $[M-H]^-$, representing the oleic fatty acid chain and a peak at *m/z* 283.2 for stearic fatty acid chain of phosphatidylcholine $[M-H]^-$ $C_{18}H_{35}O_2$. (c) Negative TOF-SIMS spectrum of the reference sample for oleic acid, showing specific peaks at *m/z* 281.2 $[M-H]^-$ $C_{18}H_{33}O_2$ and at *m/z* 282.2 $[M]^-$ $C_{18}H_{34}O_2$.

applied with a target current 0.15 pA. The high mass resolution and high mass accuracy allowed to assign chemical formulas to peaks even in the high mass range. Subsequently, mass resolved secondary ion images were acquired in burst alignment mode using Bi^{3+} (nominal mass resolution, lateral resolution 300 nm). The target current was 0.1 pA. Fields of view ranged from 176 μm × 176 μm to 500 μm × 500 μm and the pixel density was 256 × 256. The field of view is given in figure legends. Images in Figs. 3a–f, 4c–f, 5a–g and 7 were shown in the filter mode "average 2" of the IonImage program of the IONTOF-software for contrast enhancing, but no further parameters were changed. The colour scaling was the same for all images presented. The images in Figs. 5a–g and 7 were normalized to the total ion image.

3. Results and discussion

Galactosylceramide-sulfate (Gal-Cer sulfatide), a glycosphingolipid, is an integral part of the cell membrane of glial cells and nerve cells in the CNS. A reference spectrum of sulfatide (Fig. 1a) shows peaks representing molecular fragments of the sulfatide head group with different hydrocarbon chain lengths (Table 1). The negative spectrum of rat cerebellar tissue showed sulfatides (Fig. 2) as well as secondary ion peaks for palmitate at *m/z* 255 $[M-H]^-$, for oleic acid at *m/z* 281 $[M-H]^-$ and cholesterol $[M-H]^-$ at *m/z* 385.

Negative TOF-SIMS images from analysis of rat cerebellum cryostat sections are shown in Fig. 3 at a resolution of 1.95 μm/pixel and the same secondary ions are shown for high-

Table 1
Secondary ions recorded in the positive and negative mode with *m/z* calculated, *m/z* measured and the deviation in ppm

Lipid species	Formula	Calculated	Measured	*m/z* error	Designation
Negative ions					
Palmitic acid 16:0	$C_{16}H_{31}O_2$	255.232	255.234	4.9	$[M-H]^-$
Oleicacid 18:1	$C_{18}H_{33}O_2$	281.248	281.246	−6.1	$[M-H]^-$
Sulfatide 18:0	$C_{42}H_{80}SNO_{11}$	806.545	806.58	42.8	$[M-H]$
Sulfatide 22:0	$C_{46}H_{88}SNO_{11}$	862.608	862.617	9.19	$[M-H]^-$
Sulfatide H22:0	$C_{46}H_{88}SNO_{12}$	878.603	878.570	−32.72	$[M-H]^-$
Sulfatide 24:1	$C_{48}H_{90}SNO_{11}$	888.623	888.592	−31.46	$[M-H]^-$
Sulfatide 24:0	$C_{48}H_{92}SNO_{11}$	890.639	890.598	−41.11	$[M-H]^-$
Sulfatide H24:1/25:0	$C_{48}H_{90}SNO_{12}$	904.618	904.590	−28.37	$[M-H]^-$
Sulfatide H24:0	$C_{48}H_{92}SNO_{12}$	906.634	906.597	−37.02	$[M-H]^-$
Positive ions					
Phosphocholine	$C_5H_{15}PNO_4$	184.074	184.07	18.2	$[M]^+$
Cholesterol	$C_{27}H_{45}O$	385.347	385.352	12.6	$[M-H]$
Cholesterol	$C_{27}H_{45}$	369.352	369.357	13.3	$[M+H-H_2O]^+$

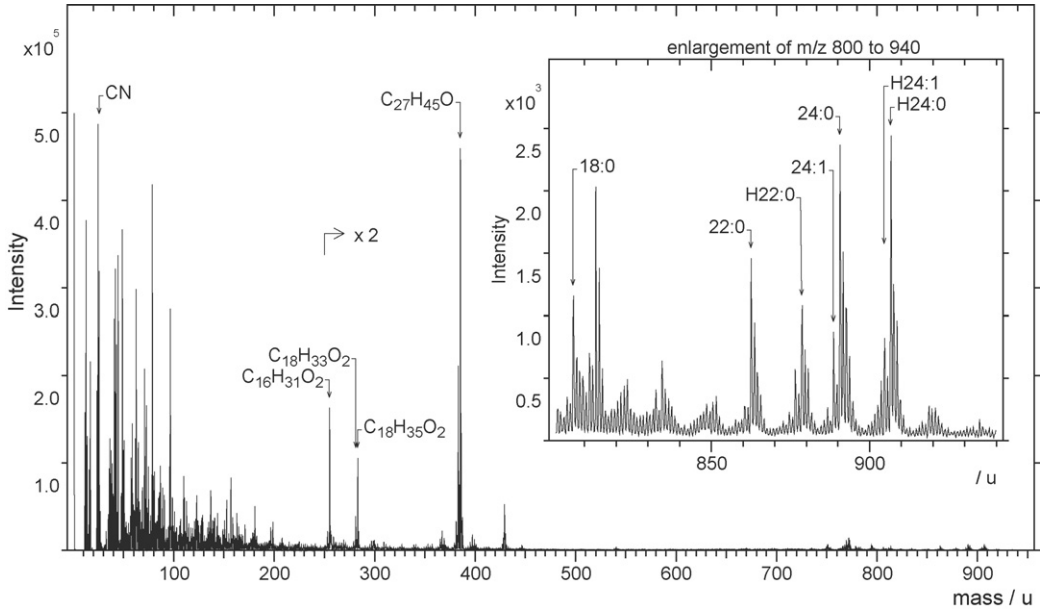

Fig. 2. Negative TOF-SIMS spectrum of rat cerebellum after plunge-freezing and cryostat sectioning with an enlargement from *m/z* 800 to 940, showing peaks of the sulfatides C18:0 at *m/z* 806.6, C22:0 at *m/z* 862.6, CH22:0 at *m/z* 878.6, C24:1 at *m/z* 888.6, C24:0 at *m/z* 890.6 and CH24:0 at *m/z* 906.6. Peaks at *m/z* 255.2 and 281.2 are seen, representing the fatty acids palmitate and oleate and the peak at *m/z* 385, showing ion distributions of cholesterol $[M-H]^-$.

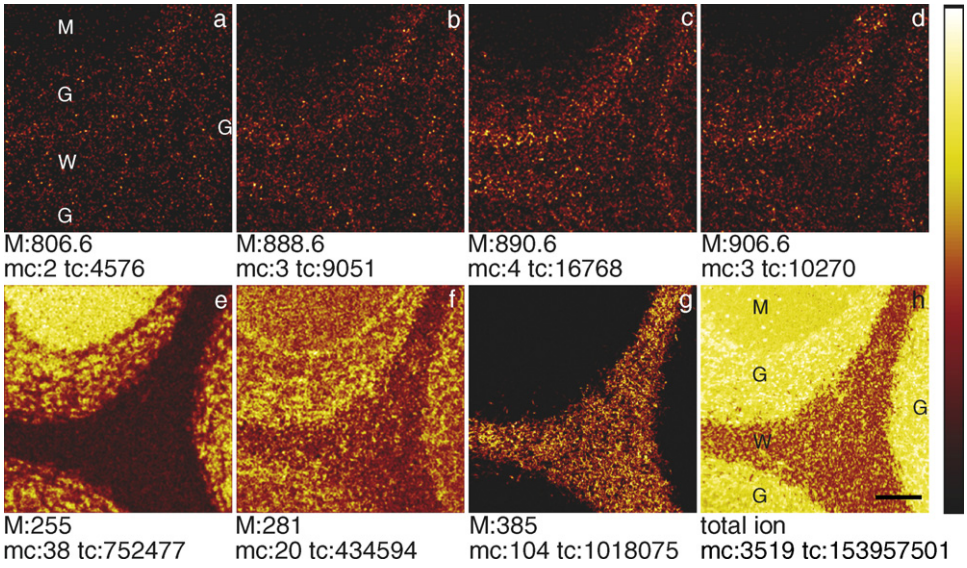

Fig. 3. Negative images of rat cerebellum analyzed with TOF-SIMS. (a–d) Sulfatides in different chain length detected at: (a) *m/z* 806.6 (C18), (b) *m/z* 888.6 (C24:1), (c) *m/z* 890.6 (C24:0) and (d) *m/z* 906.6 (CH24:0). In (e and f), secondary ion distributions were shown from peaks at: (e) *m/z* 255 (palmitate) and (f) *m/z* 281 (oleate), (g) shows the image at *m/z* 385 for cholesterol $[M-H]^-$ and (h) the total ion image. In (a and h), cell layers were assigned with W for white matter, G for the granular layer and M for molecular layer regions. The images in (a–f) are shown in the filter mode "average 2" of the IonImage program. The field of view is 500 μm × 500 μm with an image resolution of 256 × 256 pixels, the size bar = 100 μm. The colour scale ranged from black for low signal intensity to red, yellow and white for highest relative intensity of secondary ions, which is displayed by the colour scale bar on the right side. Maximum counts (mc) and total ion counts (tc) of the analyzed area are given under the each image, respectively.

pressure frozen samples of rat cerebellum in Fig. 5 (resolution 1.16 μm/pixel). Figs. 3a–d and 5a–d show molecular species of sulfatides with different hydrocarbon chain length C18 (Figs. 3a and 5a), C24:1 (Figs. 3b and 5b), C24:0 (Figs. 3c and 5c) and the hydroxylated fatty acid CH24:0 (Figs. 3d and 5d). Cholesterol (Figs. 3g and 5g) is seen in the white matter, in ribbon-shaped areas of 10–20 μm in size. The sulfatide distribution pattern are similar for all hydrocarbon chain length shown in the images, with a dot-like appearance in clusters of higher intensities mainly in white matter (W), and in the granular layer (G) regions, with higher density at the border of outer white matter to the outer granular layer. Inside the granular layer sulfatide concentration decreases in direction from white matter to molecular layer (M), where lowest intensity signals are seen. The sulfatides C24:0, CH24:0 and C24:1 showed, listed in descending order, higher secondary ion signals in TOF-SIMS analysis compared to the C18 sulfatide.

Fig. 4 gives an overview of tissue layers and components compared to its chemistry. In Fig. 4a, a Richardson tissue stain is shown. It is based on methylene blue and azan II dye, staining DNA, RNA and nuclear acids. The image shows cell nuclei in dark blue and cell cytoplasm stained in light blue for the same area, which was analyzed with TOF-SIMS on a cryosection from the same cerebellum sample. Purkinje cells were high lightened with circles. Fig. 4b shows an overlay of Fig. 4a together with the total ion image of the area analyzed with TOF-SIMS. The image shows that the cell layers co-localize to the TOF-SIMS image, revealing that lipid distributions are seen at the same borders which are defined by the cell layers seen in the Richardson stain.

The overlay image of the C24:0 sulfatide (green) and cholesterol (blue) for the cerebellum cryostat section analysis in Fig. 4c showed colour separation, where the sulfatide is seen in regions low in cholesterol inside the white matter (arrowheads). The same result could be obtained for the high-pressure frozen cerebellum sample (Fig. 4e).

Galactosylceramide-sulfate comprises 4% of the total lipid in myelin, the isolating sheets around nerve cell axons which compose the cerebellar white matter (W) [25]. Studies on Cst-deficient mice, lacking galactosylceramide-sulfate, is the most informative source of knowledge about the function of the glycolipid in brain [26]. A lack of sulfatide in mice results in desorganised termination of the lateral loops of the nodes of Ranvier, the regularly spaced gaps in the myelin sheet of nerve cell axons, and disturbed clustering of Na/K channels seen in normal mice. These findings are consistent with the data presented in this study, where the sulfatide was found localized in regions low in cholesterol, which we suggest they belong to paranodal areas of the myelin (Fig. 3). However, we also find that the Gal-Cer sulfatide is detected in the granular layer and an intense signal is seen at the border between the granular layer and the myelin. This localisation of the sulfatide to gray matter areas has also been reported by other, using TOF-SIMS for analysis of the sulfatide in cerebrum [9].

Localization of the fatty acid palmitate (C16:0) in rat cerebellum is shown in Figs. 3e and 5e, seen distributed in all three cell layers but with stronger signals in clusters of about 10–30 μm in the granular layer and highest secondary ion intensities in the molecular layer. Distribution pattern of oleate (C18:1) at *m/z* 281 is shown in Figs. 3f and 5f. Oleate shows a different distribution compared to that of palmitic acid with more intense signals in granules at the border regions of the white matter to granular layer and in linear structures at the border

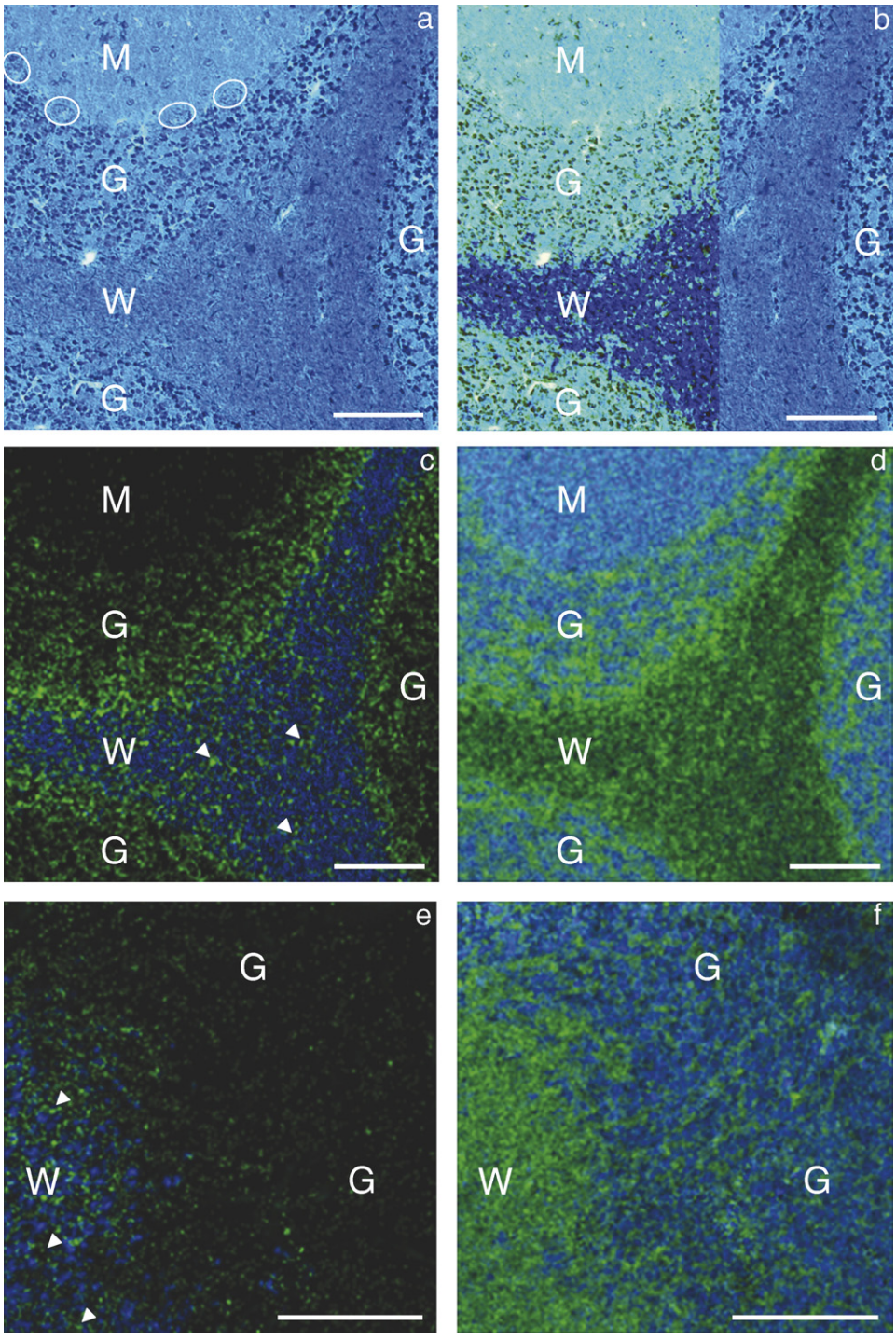

Fig. 4. Histology stain and overlays of TOF-SIMS images shown in Fig. 3 reveal localization of sulfatides and fatty acids to tissue regions. (a) Richardson tissue stain with legends for the cell layers W white matter, G granular layer and M for molecular layer. The circles highlight cerebellar purkinje cells. (b) Overlay of (a) and a part of the total ion image, seen in Fig. 3h, presented in the Photoshop overlay mode. (c) A two colour overlay image showing the sulfatide at *m/z* 890.6 in green and the ion distribution at *m/z* 385 representing cholesterol in blue from cryostat section analysis and (e) high-pressure frozen cerebellum. (d) Two colour overlay with C18 fatty acid oleate at *m/z* 281 in green and in blue the secondary ions of the C16 fatty acid palmitate at *m/z* 255 from cryostat section analysis and (f) high-pressure frozen cerebellum. *Arrowheads* point out paranodal regions in the cerebellar white mater. Image sizes for (a–d) 500 μm × 500 μm and 297 μm × 297 μm for (e–f). The scale bar = 100 μm.

of granular to molecular layers. Oleate is present in all three cell layers and the distribution pattern was in spots with higher signal intensities, which appeared irregular in shape and size in the granular layer and white matter. Both preparation methods showed this spot pattern, but secondary ion signals were seen more intense in the high-pressure frozen preparations. The molecular layer showed presence of oleate with a more even distribution.

An overlay of images from cryo-sectioned (Fig. 4d) and high-pressure-frozen cerebellum (Fig. 4f) shows the TOF-SIMS

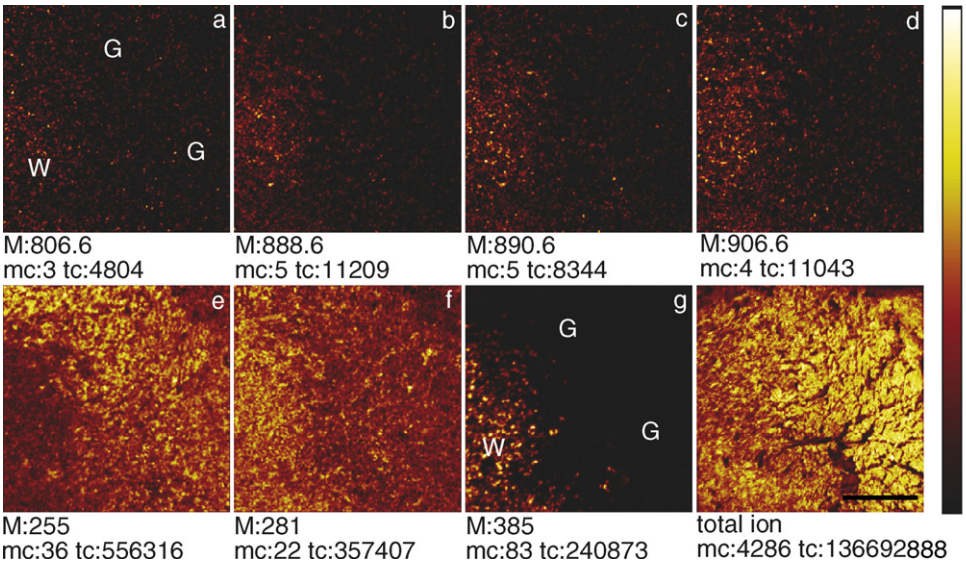

Fig. 5. Negative images of rat cerebellum analyzed with TOF-SIMS. (a–d) Sulfatides in different chain length detected at: (a) *m/z* 806.6 (C18), (b) *m/z* 888.6 (C24:1), (c) *m/z* 890.6 (C24:0) and (d) *m/z* 906.6 (CH24:0). In (e–f), secondary ion distributions were shown from peaks at (e) *m/z* 255 (palmitate) and f) *m/z* 281 (oleate), (g) shows the image at *m/z* 385 for cholesterol $[M-H]^-$ and (h) the total ion image. In (a and h), cell layers were assigned with W for white matter and G for the granular layer. The molecular layer is not seen. The images in (a–g) were shown in the filter mode "average 2" of the IonImage program and normalized to the total ion image. The field of view is 297 μm × 297 μm with an image resolution of 256 × 256 pixels, the size bar = 100 μm. The colour scale ranged from black for low signal intensity to red, yellow and white for highest relative intensity of secondary ions, which is displayed by the colour scale bar on the right side. Maximum counts (mc) and total ion counts (tc) of the analyzed area are given under the each image, respectively.

images of palmitate at *m/z* 255 and oleate at *m/z* 281. Since both molecular species are seen all-over in the cerebellar layers, though with different distribution pattern, the images merge slightly for white matter regions and regions in the granular layer, but show mainly colour separation and therefore a different distribution pattern.

The heterogeneous localization of fatty acids among areas in the cerebellum seen in the present study is, to the best of our knowledge, a new finding. The interpretation is that cells may select fatty acids for their synthesis of phospholipids and spingolipids in the same manner that different headgroups of lipids are found in different membranes [27]. Reference samples of phosphatidylcholine (Fig. 1b) and oleic acid (Fig. 1c) showed specific fatty acid peaks at *m/z* 255 for palmitate $[M]^-$ and at *m/z* 281 for oleate $[M]^-$, which were also seen in the tissue spectrum (Fig. 2). The fatty acids have probably been cleaved from phospholipids, since these molecules tend to form fragment patterns containing molecular fatty acids and intact headgroups (Fig. 1b). Sphingolipids show a more complex pattern of fragmentation [12] without formation of free fatty acids. As reported earlier by our group, the phosphatidylcholine headgroup at *m/z* 184 is evenly distributed, all-over the granular and the molecular cell layer, with some clusters of higher intensities inside the white matter [12]. The fact that we see different distribution pattern of fatty acids of different chain lengths compared to the headgroup of the molecule, most probably reflects cellular selection of fatty acids in the synthesis of phospholipids. This selection may either be due to selective uptake of fatty acids by fatty acid transport proteins (FATPs) or, more probably, due to selective expression of enzymes synthesizing phospholipids in the ER [27].

Mouse intestine samples, taken from control mice and after 8 h treatment with 25 μg cholera toxin (CT), were plunge frozen, cut with a cryostat and analyzed with TOF-SIMS for lipid chemistry. Positive TOF-SIMS spectra in high mass resolution of control and treated mouse intestine samples were shown in Fig. 6. The lower spectrum (CT treated) is displayed in reverse direction. A significant peak at *m/z* 184, representing the phosphocholine head group of sphingomyelin and phosphatidylcholine $[C_5H_{15}PNO_4]^+$, and the peak at *m/z* 369, which was used for imaging the distribution of cholesterol $[M + H\text{-}H_2O]^+$ $C_{27}H_{45}$, were seen in both spectra. The spectra comparison showed significant increased cholesterol concentrations for the cholera toxin treated intestine samples. Fig. 7a–c shows positive TOF-SIMS images on the analysis of mouse control intestine in a resolution of 0.79 μm/pixel. Fig. 7d–f gives information on the ion distribution pattern in cholera toxin treated mouse intestine samples in a resolution of 0.67 μm/pixel. In Fig. 7a, the TOF-SIMS image of phosphocholine at *m/z* 184 is shown. Intestine villi reveal high secondary ion intensities of phosphocholine, but weaker signals are seen in cell nucleus regions (*arrows*) and at the enterocyte brush border on the lumen side (L). Cholesterol, at *m/z* 369, is seen in lower concentrations (Fig. 7b), but as seen in the overlay (Fig. 7c) of phosphocholine (red) and cholesterol (green), it is localized to the lumen side, at the brush border area of enterocytes, and to intestine cell nuclei. The phosphocholine distribution (Fig. 7d) in cholera toxin treated intestine is not as distinct as in control tissue, but in the same distribution pattern with high ion intensities in the villi and lower concentrations in the lumen (L) and to the nuclear regions of the enterocytes. Cholesterol (Fig. 7e) is seen in significantly higher concentrations than in control intestine samples. The overlay in Fig. 7f

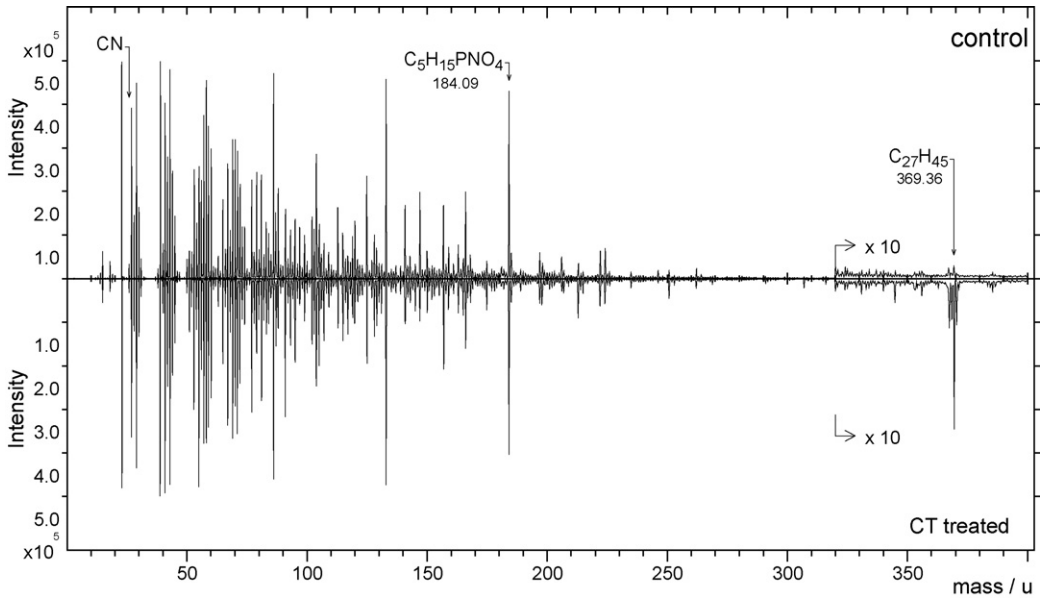

Fig. 6. Positive TOF-SIMS spectrum of mouse intestine samples prepared by plunge-freezing and cryostat sectioning. The upper spectrum shows secondary ions from the untreated control sample and the lower spectrum, seen in reverse view, show results of the mouse intestine sample treated with choleratoxin for 8 h. A peak at *m/z* 184, representing the phosphocholine headgroup and a peak at *m/z* 369, showing the cholesterol fragment $[M+H-H_2O]^+$, were pointed out.

shows accumulation of cholesterol (green) in the brush border area of enterocytes after cholera toxin treatment.

Localization of cholesterol to the brush border area of the enterocytes may be due either to the presence of cholesterol-rich lipid rafts present on the microvilli [28], or the cholesterol is bound to scavenger receptors (SR-BI) as a part of the process of cholesterol uptake by the intestines [29]. Exposure to cholera toxin was found to cause a profound redistribution of choles-

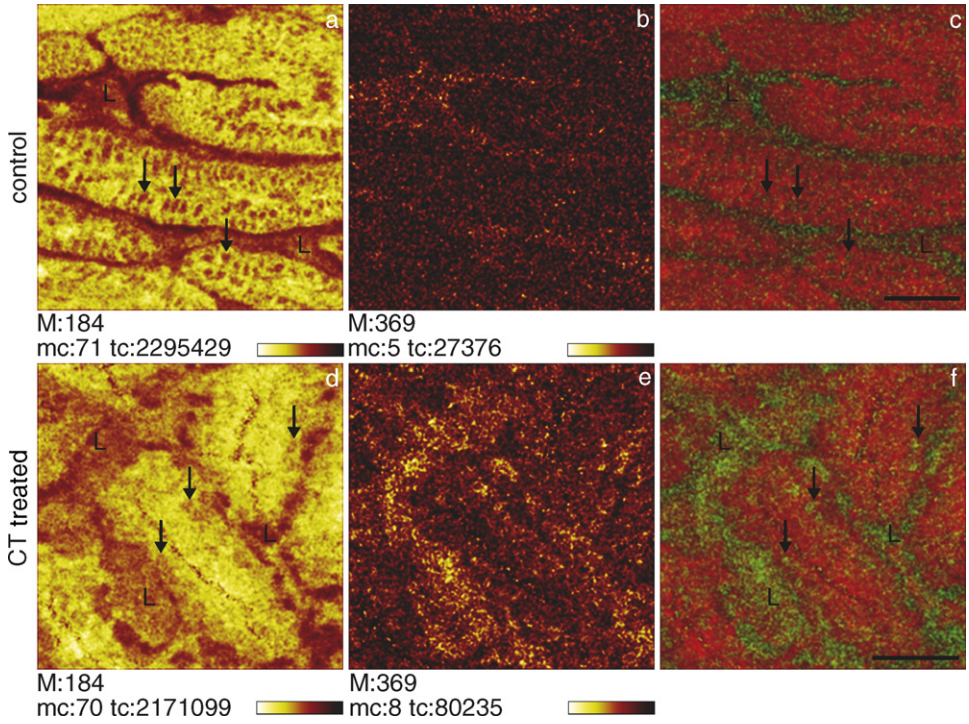

Fig. 7. Positive TOF-SIMS ion images of intestine from control and choleratoxin (CT) treated mice after 8 h. The tissue was prepared by plunge-freezing and cryostat sectioning. Images (a, b, d and e) have been normalized to the total ion image. All images were shown in the filter mode "average 2" of the IonImage program, in an image resolution of 256 × 256 pixels. The field of view = 201 μm × 201 μm for images (a–c) and 176 μm × 176 μm for images (d–f). (a and d) Ion distributions at *m/z* 184, representing the phosphocholine headgroup $C_5H_{15}PNO_4$. (b and e) Secondary ion images at *m/z* 369, representing the cholesterol fragment $[M+H-H_2O]^+$. (c and f) Two colour overlay of phosphocholine distribution pattern at *m/z* 184 in red and the cholesterol signal at *m/z* 369 in green. *Arrows* show cell nuclei regions with lower phosphocholine concentrations, L points out the lumen. Maximum counts (mc) and total ion counts (tc) of the analyzed area are given under the each image, respectively.

terol in the intestinal villi. After 8 h, the cholesterol was found below the epithelium, apparently in the interstitium of the villi. As judged from the tissue spectra, the amount of cholesterol increases during eight hours of exposure to cholera toxin. The fraction of cholesterol found in the nuclei of enterocytes also seems to increase after exposure to cholera toxin.

Both tissue preparation methods (see Sections 2.2.1 and 2.2.2) are shown to be suitable tools for the study of lipid localization in tissues and for different biological questions by TOF-SIMS. Plunge-freezing is a quite simple method, but though the tissue is not fixed or cryo-preserved, we cannot avoid the crystallization of water to ice and have to be aware that ion redistributions can occur. This is acceptable for analysis at lower resolution and it should not effect the results for the compound localization. High-pressure freezing in contrast, preserves the tissue in its natural state by formation of amorphous ice without a liquid phase and therefore ice crystallization and ion or lipid redistribution, does not occur. Thus, analysis of tissue in higher resolution is possible. One disadvantage of the high-pressure freezing method is that the surface topography is not completely plane. Freeze-fracturing creates a randomly fractured surface of the sample, which we compensated for by normalization of the images to the total ion image.

4. Conclusion

The power of detecting and imaging lipids in tissues with TOF-SIMS, is a big step forward, for basic biochemical, biological and biomedical research. In this work, we show examples of lipids that play a crucial role in cell composition cell signalling and metabolism. Tissue preparation is a pivotal step, when analysing the tissue chemistry under vacuum conditions. Two suitable preparation procedures for imaging TOF-SIMS, were presented.

Considering the fact that new kinds of data are made available, we anticipate that imaging TOF-SIMS may reach the same importance in biological sciences as fluorescence microscopy and electron microscopy have today.

Acknowledgements

This study was supported by the Swedish National Research Council (NT). Mrs Elke Tallarek at Tascon GmbH is acknowledged for her skilled work. Thanks to Prof. Jan Holmgren at our department for contributing with the exposure of mice to cholera toxin.

References

[1] D.E. Vance, J.E. Vance, Biochemistry of lipids, lipoproteins and membranes, fourth ed., Elsevier Science B.V., Amsterdam, 2002.
[2] B.L. Peterson, B.S. Cummings, Biomed. Chromatogr. 20 (3) (2006) 227.
[3] E.J. Lesnefsky, M.S. Stoll, P.E. Minkler, C.L. Hoppel, Anal. Biochem. 285 (2) (2000) 246.
[4] D.S. Lester, J.L. Olds, B.G. Schreurs, D. McPhie, C.R. Bramham, D.L. Alkon, Neuroimage 1 (4) (1994) 264.
[5] L. Kuerschner, C.S. Ejsing, K. Ekroos, A. Shevchenko, K.I. Anderson, C. Thiele, Nat. Methods 2 (1) (2005) 39.
[6] S. Parry, N. Winograd, Anal. Chem. 77 (24) (2005) 7950.
[7] A.F. Altelaar, I. Klinkert, K. Jalink, R.P. de Lange, R.A. Adan, R.M. Heeren, S.R. Piersma, Anal. Chem. 78 (3) (2006) 734.
[8] D. Touboul, A. Brunelle, F. Halgand, S. De La Porte, O. Laprevote, J. Lipid Res. 46 (7) (2005) 1388.
[9] P. Sjovall, J. Lausmaa, B. Johansson, Anal. Chem. 76 (15) (2004) 4271.
[10] L.A. McDonnell, R.M. Heeren, R.P. de Lange, I.W. Fletcher, J. Am. Soc. Mass Spectrom. (2006).
[11] A. Brunelle, D. Touboul, O. Laprevote, J. Mass Spectrom. 40 (8) (2005) 985.
[12] K. Borner, H. Nygren, B. Hagenhoff, P. Malmberg, E. Tallarek, J.E. Mansson, Biochim. Biophys. Acta 1761 (3) (2006) 335.
[13] D. Touboul, F. Kollmer, E. Niehuis, A. Brunelle, O. Laprevote, J. Am. Soc. Mass Spectrom. 16 (10) (2005) 1608.
[14] H. Nygren, P. Malmberg, C. Kriegeskotte, H.F. Arlinghaus, FEBS Lett. 566 (1–3) (2004) 291.
[15] L.A. McDonnell, S.R. Piersma, A.F. MaartenAltelaar, T.H. Mize, S.L. Luxembourg, P.D. Verhaert, J. van Minnen, R.M. Heeren, J. Mass Spectrom. 40 (2) (2005) 160.
[16] E.B. Monroe, J.C. Jurchen, J. Lee, S.S. Rubakhin, J.V. Sweedler, J. Am. Chem. Soc. 127 (35) (2005) 12152.
[17] A. Benninghoven, Surf. Sci. 299 (1994) 246.
[18] P.J. Todd, J.M. McMahon, R.T. Short, C.A. McCandlish, Anal. Chem. 69 (17) (1997) 529A.
[19] D. Touboul, F. Halgand, A. Brunelle, R. Kersting, E. Tallarek, B. Hagenhoff, O. Laprevote, Anal. Chem. 76 (6) (2004) 1550.
[20] F. Kollmer, Appl. Surf. Sci. 231-232 (2004) 153.
[21] D. Studer, W. Graber, A. Al-Amoudi, P. Eggli, J. Microsc. 203 (Pt 3) (2001) 285.
[22] A. Warley, J.N. Skepper, J. Microsc. 198 (Pt 2) (2000) 116.
[23] J.-E. Månsson, L. Svennerholm, Clin. Chim. Acta 126 (1982) 127.
[24] L. Svennerholm, K. Boström, P. Fredman, J.-E. Månsson, B.-M. Rynmark, Biochim. Biophys. Acta 1128 (1992) 1.
[25] I. Ishizuka, Prog. Lipid Res. 36 (4) (1997) 245.
[26] K. Honke, Y. Zhang, X. Cheng, N. Kotani, N. Taniguchi, Glycoconj. J. 21 (1-2) (2004) 59.
[27] A.L. Henneberry, M.M. Wright, C.R. McMaster, Mol. Biol. Cell 13 (9) (2002) 3148.
[28] H.T. Nguyen, A.B. Amine, D. Lafitte, A.A. Waheed, C. Nicoletti, C. Villard, M. Letisse, V. Deyris, M. Roziere, L. Tchiakpe, C.D. Danielle, L. Comeau, A. Hiol, Biochem. Biophys. Res. Commun. 342 (1) (2006) 236.
[29] E. Levy, D. Menard, I. Suc, E. Delvin, V. Marcil, L. Brissette, L. Thibault, M. Bendayan, J. Cell Sci. 117 (Pt 2) (2004) 327.